Growth Model for Pulsed-Laser Deposited Perovskite Oxide Films *

WANG Xu(王旭)[1], FEI Yi-Yan(费义艳)[2], ZHU Xiang-Dong(朱湘东)[1,2**], LU Hui-Bin(吕惠宾)[1],
YANG Guo-Zhen(杨国桢)[1]

[1]Beijing National Laboratory for Condensed Matter Physics, Institute of Physics, Chinese Academy of Sciences,
Beijing 100080
[2]Department of Physics, University of California at Davis, Davis, California 95616, USA

We present a multi-level growth model that yields some of the key features of perovskite oxide film growth
as observed in the reflection high energy electron diffraction (RHEED) and ellipsometry studies. The model
describes the effect of deposition, temperature, intra-layer transport, interlayer transport and Ostwald ripening
on the morphology of a growth surface in terms of the distribution of terraces and step edges during and after
deposition. The numerical results of the model coincide well with the experimental observation.

Growth of crystalline films on solids is one of the major methods for making novel materials or material forms. The structural quality of a grown film is characterized by the distribution of terraces and step edges. During and after deposition, such a distribution is a function of growth conditions and kinetics such as deposition flux, substrate temperature, intra-layer transport (motion on a terrace), interlayer transport (crossing between two neighbouring terraces), and Ostwald ripening.[1−3] Suitable kinetic models with a set of tractable parameters enable experimental optimization and control of thin film growth. Monte Carlo simulations[4,5] and molecular dynamics calculations[6] are examples of numerical models. Analytical models involve rate equations[7,8] and thus lend itself to a more convenient exploration of parameters that are most likely responsible to certain growth behaviours. So far few analytical models have explicitly taken into account of the Ostwald ripening[1,3] during and after deposition. The goodness of a model can be judged by how well its prediction compares with experimental observation. Experimentally a film morphology can be characterized in situ using reflection high energy electron diffraction (RHEED),[9−11] surface x-ray diffraction (SXRD),[12,13] thermal atom scattering,[14] or optical reflection.[15−18] The intensities of RHEED or SXRD can be quantitatively related to the distribution of terraces of a growth surface.[7] The intensity of a specularly reflected thermal helium atom beam or an optical beam varies linearly with the surface atoms or unit cells at step edges.[13,19]

In this Letter, we describe a multi-level (i.e., multi-terrace) growth model based on a birth-death model [8] In our model we consider the Ostwald ripening during and after deposition as the effect is prevalent in the growth of perovskite oxides. The model yields some general features that are observable in our recent RHEED and optical studies of perovskite oxide film growth. This is the first step to use such a model to analyze and predict the growth behaviour.[20]
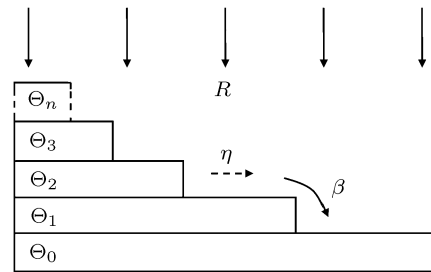

Fig. 1. An n-level (terrace) growth model. $\Theta_0 \leq j \leq n$ is the coverage of the j-th terrace that is at distance $j \times d$ from the substrate surface. R is the deposition rate in units of monolayers per second, β is the fraction of monomeric unit cells on a terrace that makes to the neighbouring lower terrace and thus includes the effect of the interlayer transport. Here η characterizes the Ostwald ripening effect that causes an upper terrace to disintegrate when the coverage of the lower terrace is not full.

Figure 1 shows a distribution of n terraces (i.e., n-level model) during and after growth. Let d be the thickness (i.e., the height) of the unit cell or the interlayer spacing. $\Theta_0 \leq j \leq n$ is the coverage or footprint of the j-th terrace that is $j \times d$ from the substrate surface. We consider four kinetic processes that occur during growth: deposition, intra-layer transport, interlayer transport, and dissociation of islands due to Gibbs-Thompson effect or Ostwald ripening. The deposition rate R is the number of monolayers deposited per unit time. $\tau = 1/R$ is the time it takes to deposit one monolayer of the material. We assume that the intra-layer transport is efficient so that the mass transfer is rate-limited by the interlayer transport and

---

the Gibbs–Thompson or Ostwald ripening effect. The latter causes detachment of unit cells from edges of terraces. The net mass transfer from the $(j+1)$-th terrace to the j-th terrace due to the Ostwald ripening effect alone is the diffusive flux leaving the perimeter of the $(j+1)$-th terrace multiplied by the number density of the upper terrace islands. For simplicity, we assume that the rate of detachment in units of monolayers per second is proportional to the coverage of the $(j+1)$-th terrace with the proportionality constant η being only a function of temperature. For interlayer transport, we assume that a fixed fraction β of newly deposited unit cells on the j-th terrace and the detached unit cells from the $(j+1)$-th terrace makes it to the $(j-1)$-th terrace if the latter is not yet full. β is a function of temperature and includes the effect of step edge barrier and surface diffusion barrier. The remaining fraction $(1-\beta)$ stays on the j-th terrace and adds to the $(j+1)$-th terrace. With these assumptions, we can write down the rate equations for the coverage of each terrace as follows:[20]

$$\frac{d\Theta_1}{dt} = R(\Theta_0 - \Theta_1) + \beta[R(\Theta_1 - \Theta_2)$$
$$+ \eta\Theta_2]H(1 - \Theta_1),$$
$$\frac{d\Theta_j}{dt} = R(\Theta_{j-1} - \Theta_j) + \beta[R(\Theta_j - \Theta_{j+1})$$
$$+ \eta\Theta_{j+1}]H(1 - \Theta_j) - \beta[R(\Theta_{j-1} - \Theta_j)$$
$$+ \eta\Theta_j]H(1 - \Theta_{j-1}), (1 < j < n)$$
$$\frac{d\Theta_n}{dt} = R(\Theta_{n-1} - \Theta_n) + R\Theta_n - \beta[R(\Theta_{n-1}$$
$$- \Theta_n) + \eta\Theta_n]H(1 - \Theta_{n-1}),$$
$$\Theta_{n+1} = 0, \tag{1}$$

where $H(u)$ is the Heaviside unit step function: $H(u > 0) = 1$, while $H(u \leq 0) = 0$. It ensures that when a lower terrace is filled, the transfer of material from the neighbouring upper terrace is stopped. For a distribution of Θ_j, the mean squared roughness is given by

$$\Delta^2 = \sum_{j=0}^{n}(j - t/\tau)^2(\Theta_j - \Theta_{j+1}). \tag{2}$$

From Eq. (2), such a growth model can be compared to the thin film morphology as determined with specular thermal helium atom reflection or oblique-incidence optical reflection. To compare the prediction of a growth model with RHEED or SXRD measurements under the condition that the reflected wavelets from two neighbouring terraces are Φ out of phase, one computes the following from Θ_j,[7]

$$I = I_{\max}\Big|\sum_{j=0}(\Theta_j - \Theta_{j+1})e^{i(j\Phi)}\Big|^2$$
$$= I_{\max}\Big|\sum_{j=0}\theta_j e^{i(j\Phi)}\Big|^2. \tag{3}$$

When $\beta = 0$ and $\eta = 0$ so that interlayer transport and island dissociation are effectively prohibited, the film surface during a continuous deposition quickly becomes rough. For illustration we consider a 16-level model ($n = 16$). Figure 2 shows the evolution of terraces $\Theta_j(t)$, specular RHEED intensity (from Eq. (3)), and the rms roughness $r \equiv \sqrt{\Delta^2}$ (from Eq. (2)) with the initial condition of $\Theta_0(0) = 1$, $\Theta_j(0) = 0(0 < j \leq 16)$. The specular RHEED and SXRD intensity under the anti-phase condition with $\Phi = 180°$ diminishes rapidly while the rms roughness increases monotonically.

When $\beta = 1$ and $\eta \gg 1$, the unit cells that are deposited on a terrace or detached from ist upper neighbouring terraces all make it to its lower neighbouring terrace and we have a perfect layer-by-layer growth. In this case, $\Theta_0 = 1$, $\Theta_1 = t/\tau$, $\Theta_{j>1} = 0$, $I(t) = I_{\max}[1 - (2t/\tau)]^2 + 4(t/\tau)(1 - t/\tau)\cos^2(\Theta/2)$ with the minimum of $I_{\min} = I_{\max}\cos^2(\Phi/2)$ occurring at one-half monolayer. Figure 3 shows the distribution of terraces, specular RHEED reflection, and rms roughness during a continuous deposition with $\beta = 1, \eta \gg 1$, and $\Theta = 180°$. The coverage of a terrace begins to increase only when its lower neighbouring terrace is full. The rate of increase is $R = 1/\tau$. The specular RHEED or SXRD intensity is periodic with a time period of τ. Within the time period $I(t) = I_{\max}[1 - (2t/\tau)]^2$ and $r \equiv \sqrt{\Delta^2} \sim \sqrt{(t/\tau[1 - (t/\tau)])}$.

When β is less than unity yet not zero, the interlayer transport is insufficient to sustain a perfect layer-by-layer growth. As shown in Fig. 4, the growth surface consists of more than 4 incomplete terraces. The specular RHEED or SXRD decreases but to a level above zero with a small oscillatory component on. The rms roughness increases to an asymptotic level with a reduced oscillatory component. The magnitudes of oscillation for RHEED or SXRD and for rms roughness decrease with decreasing β. Remaining oscillations in RHEED or SXRD and in rms roughness indicate a quasi-layer-by-layer growth. We note that interlayer transport (characterized by β) is most important in deciding whether the growth proceeds in layer-by-layer mode or rough growth mode. In these calculations, η is set to 0.05.

The Ostwald ripening as characterized by η is the dominating process during post-deposition annealing. In an oxide growth using pulsed-laser ablation deposition method, the deposition is often interrupted (intermittent growth) so that the growth surface and its oxygen content can be restored through annealing. In our present growth model, we can compute the distribution of terrace coverage after as well as during the deposition and compare the results with in-situ RHEED or optical reflection measurements.
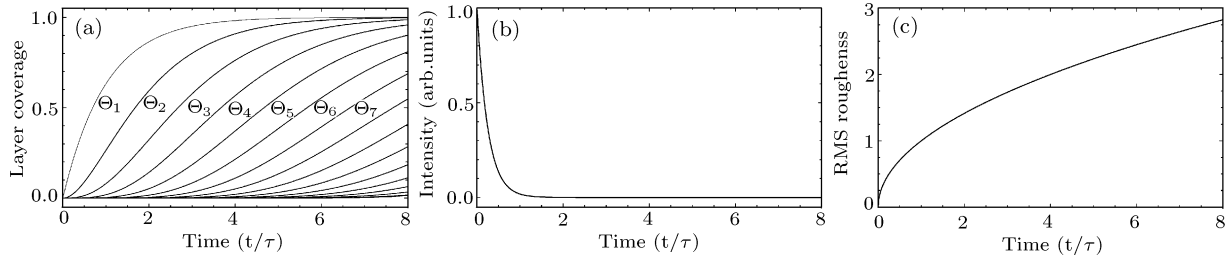
Fig. 2. Distribution of 16 terraces, the corresponding rms roughness r, and the specular RHEED diffraction intensity $I(t)$ during a continuous deposition calculated from Eq. (1) with $\beta = 0$ and $\eta = 0$.
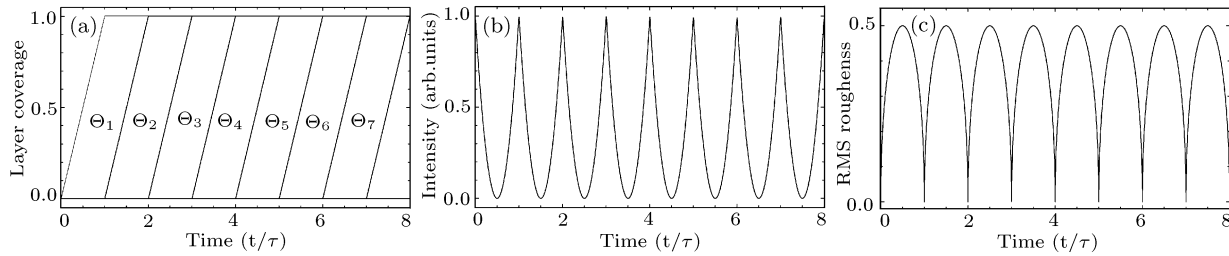

Fig. 3. Distribution of 16 terraces, the rms roughness r, and the specular RHEED diffraction intensity $I(t)$ during a continuous deposition calculated from Eq. (1) with $\beta = 1$ and $\eta \gg 1$. The growth corresponds to a perfect layer-by-lay growth.
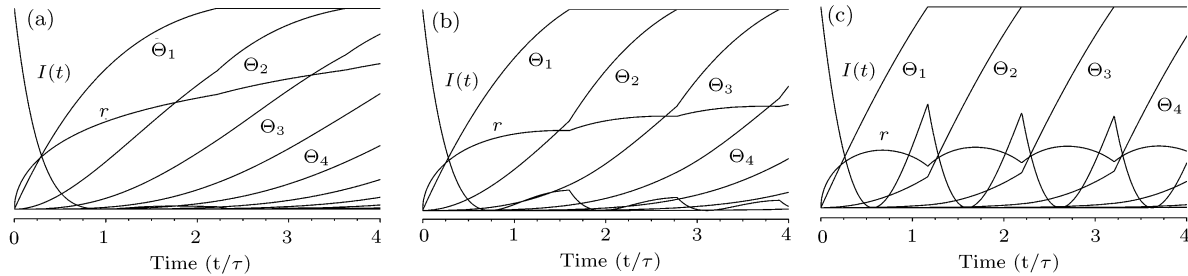

Fig. 4. Distribution of 16 terraces, the rms roughness r, and the specular RHEED diffraction intensity $I(t)$ during a continuous deposition calculated from Eq. (1) with $\eta = 0.5$: (a) $\beta = 0.3$, (b) $\beta = 0.5$, (c) $\beta = 0.8$.
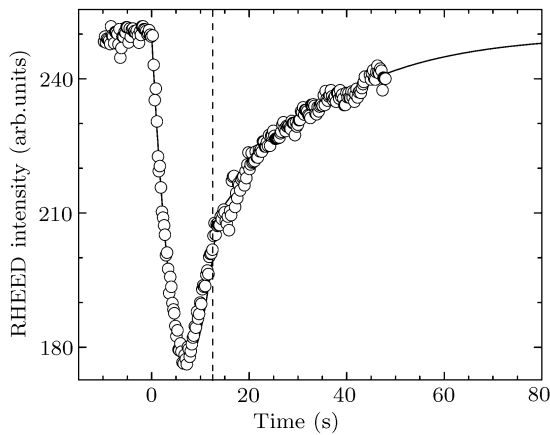

Fig. 5. Experimental RHEED intensity measured during an intermittent growth of Nb:SrTiO$_3$ monolayer on SrTiO$_3$(100) in a laser molecular-beam epitaxy chamber. The deposition rate is $R = 0.105\,\text{ML/s}$. The substrate temperature is 715°C. The solid line is the calculated RHEED intensity using the 16-level model with $\beta = 0.82$ and $\eta = 0.7$.

We apply this growth model to an intermittent growth of Nb-doped SrTiO$_3$ on SrTiO$_3$(100) under pulsed laser deposition condition. In intermittent growth, we deposit one monolayer equivalent of the oxide material and let the as-deposited film anneal for a period of time before further deposition. The experiment was performed in a laser-MBE chamber with a base pressure of $1.0 \times 10^{-5}\,\text{Pa}$. The surface morphology was monitored with in-situ RHEED. The substrate temperature was set at 715°C during deposition. In Fig. 5, we display the RHEED signal (open circles) during one cycle of an intermittent growth. The dashed line marks the end of deposition. The RHEED signal did not recover fully after deposition, indicating that the growth was not of a perfect layer-by-layer mode. The deposited Nb:SrTiO$_3$ unit cells on SrTiO$_3$(100) are distributed over at least two incomplete terraces. In our model, this corresponds to an epitaxial growth with $\beta < 1$. The subsequent recovery of the RHEED signal was driven by Ostwald

ripening. The solid line is the calculated RHEED using Eq. (1) and Eq. (3) with $\beta = 0.82$ and $\eta = 0.70$. The calculation fits the experimental results very well. From Fig. 4(c), we should expect to observe a reduced and yet still significant oscillation in RHEED intensity in a continuous deposition of Nb:SrTiO$_3$. In Fig. 6, we show the experimentally measured RHEED intensity during a continuous deposition of Nb:SrTiO$_3$ on SrTiO$_3$(100) at a rate of $R = 0.105$ ML/sec. The temperature of the SrTiO$_3$(100) substrate during the deposition was 620°C. The incomplete recovery to the pre-deposition level and the reduced oscillation of the RHEED intensity is consistent with a growth with $\beta < 1$ at low growth temperatures.
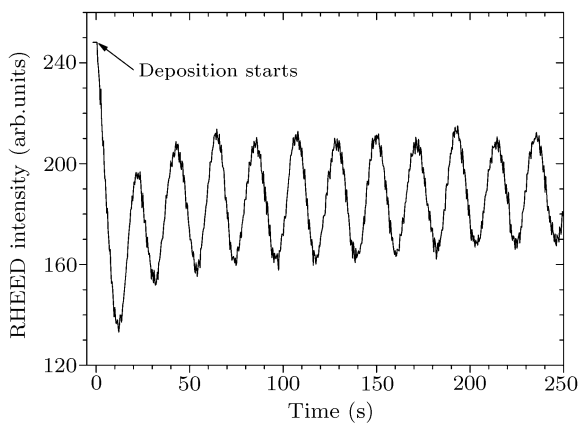

Fig. 6. Experimental RHEED intensity measured during a continuous deposition of Nb:SrTiO$_3$ on SrTiO$_3$(100) in a laser molecular-beam epitaxy chamber. The deposition rate is $R = 0.105$ ML/s. The substrate temperature is 620°C.

We should caution that generally η may be a complex function of surface morphology including the radius of curvature of a terrace. Since Eq. (1) is solved numerically, this adds little to the numerical complexity of the model.

In conclusion, we have presented a simple growth model that includes the effects of deposition rate R, interlayer transport β, and Ostwald ripening η. The numerical nature of this model can afford to include more realistic and thus more complex surface morphology dependence.

References

[1] Zinke-Allmang M, Feldman L C and Grabow M H 1992 *Surf. Sci. Rep.* **16** 377
[2] Tersoff J, Denier van der Gon A W and Tromp R M 1994 *Phys. Rev. Lett.* **72** 266
[3] Ostwald W 1900 *Z. Phys. Chem.* (Leipzig) **43** 495
[4] Clarke S and Vvedensky D D 1987 *Phys. Rev. Lett.* **58** 2235
[5] Schneider M, Rahman A and Schuller I K 1985 *Phys. Rev. Lett.* **55** 604
[6] Šmilauer P and Vvedensky D D 1993 *Phys. Rev.* B **48** 17603
[7] Cohen P I, Petrich G S, Pukite P R, Whaley G J and Arrott A S 1989 *Surf. Sci.* **216** 222
[8] van der Vegt H A, van Pinxteren H M, Lohmeier M and Vlieg E 1992 *Phys. Rev. Lett.* **68** 3335
[9] Neave J H, Joyce B A, Dobson P J and Norton N 1983 *Appl. Phys.* A **31** 1
[10] Sakamoto T, Kawai N J, Nakagawa T, Ohta K, Kojima T and Hashiguchi G 1986 *Surf. Sci.* **174** 651
[11] Koster G, Kropman B L, Rijnders G J H M, Blank D H A and Rogalla H 1998 *Appl. Phys. Lett.* **73** 2920
[12] Vlieg E, Denier van der Gon A W, van der Veen J F, Macdonald J E and Norris C 1988 *Phys. Rev. Lett.* **61** 2241
[13] Eres G, Tischler J Z, Yoon M, Larson B C, Rouleau C M, Lowndes D H and Zschack P 2002 *Appl. Phys. Lett.* **80** 3379
[14] Poelsema B and Comsa G 1989 *Scattering of Thermal Energy Atoms from Disordered Surfaces* (Berlin: Springer)
[15] JÖnsson J, Deppert K, Jeppesen S, Paulsson G, Samuelson L and Schmidt P 1990 *Appl. Phys. Lett.* **56** 2414
[16] Reinhardt F, Richter W, Müller A B, Gutsche D, Kurpas P, Ploska K, Rose K C and Zorn M 1993 *J. Vac. Sci. Technol.* B **11** 1427
[17] Kobayashi N and Horikoshi Y 1990 *Jpn. J. Appl. Phys.* **29** L702
[18] Fei Y Y, Zhu X D, Liu L F, Lu H B, Chen Z H and Yang G Z 2004 *Phys. Rev.* B **69** 233405
[19] Zhu X D 2004 *Phys. Rev.* B **69** 115407
[20] Zhu X D, Fei Y Y, Wang X, Lu H B and Yang G Z 2007 *Phys. Rev.* B **75** 245434